AGU PUBLICATIONS

JGR

Journal of Geophysical Research: Biogeosciences

RESEARCH ARTICLE
10.1002/2015JG003162

Key Points:
- Coupled modeling of hyporheic flow and temperature-dependent N reactions
- Hyporheic zone N sink/source function depends on temperature
- Hyporheic zone N sink/source function depends on $[NO_3^-]/[NH_4^+]$ ratio

Correspondence to:
L. Zheng,
lizhizheng@utexas.edu

Citation:
Zheng, L., M. B. Cardenas, and L. Wang (2016), Temperature effects on nitrogen cycling and nitrate removal-production efficiency in bed form-induced hyporheic zones, *J. Geophys. Res. Biogeosci.*, *121*, doi:10.1002/2015JG003162.

Received 23 JUL 2015
Accepted 21 MAR 2016
Accepted article online 27 MAR 2016

Temperature effects on nitrogen cycling and nitrate removal-production efficiency in bed form-induced hyporheic zones

Lizhi Zheng[1], M. Bayani Cardenas[1], and Lichun Wang[1]

[1]Geological Sciences, University of Texas at Austin, Austin, Texas, USA

Abstract Hyporheic flow in aquatic sediment controls solute and heat transport thereby mediating the fate of nutrients and contaminants, dissolved oxygen, and temperature in the hyporheic zone (HZ). We conducted a series of numerical simulations of hyporheic processes within a dune with different uniform temperatures, coupling turbulent open channel fluid flow, porous fluid flow, and reactive solute transport to study the temperature dependence of nitrogen source/sink functionality and its efficiency. Two cases were considered: a polluted stream and a pristine stream. Sensitivity analysis was performed to investigate the influence of stream water $[NO_3^-]/[NH_4^+]$. The simulations showed that in both cases warmer temperatures resulted in shallower denitrification zones and oxic-anoxic zone boundaries, but the trend of net denitrification rate and nitrate removal or production efficiency of the HZ for these two cases differed. For both cases, at high $[NO_3^-]/[NH_4^+]$, the HZ functioned as a NO_3^- sink with the nitrate removal efficiency increasing with temperature. But at low $[NO_3^-]/[NH_4^+]$ for the polluted stream, the HZ is a NO_3^- sink at low temperature but then switches to a NO_3^- source at warmer temperatures. For the pristine stream case, the HZ was always a NO_3^- source, with the NO_3^- production efficiency increasing monotonically with temperature. In addition, although the interfacial fluid flux expectedly increased with increasing temperature due to decreasing fluid viscosity, the total nitrate flux into the HZ did not follow this trend. This is because when HZ nitrification is high, uniformly elevated $[NO_3^-]$ lowers dispersive fluxes into the HZ. We found that there are numerous confounding and interacting factors that combined to lead to the final temperature dependence of N transformation reaction rates. Although the temperature effect on the rate constant can be considered as the dominant factor, simply using the Arrhenius equation to predict the reaction rate would lead to incomplete insight by ignoring the changes in interfacial fluid and solute fluxes and reaction zone areas. Our study shows that HZ temperature and stream $[NO_3^-]/[NH_4^+]$ are key controls for HZ sink/source functions.

1. Introduction

Excess bioavailable nitrogen in stream waters, especially nitrate (NO_3^-), is a significant concern because it is a drinking water pollutant and causes eutrophication that threatens aquatic ecosystems [*Boano et al.*, 2014; *Galloway et al.*, 2003; *Groffman et al.*, 2005]. Previous studies have shown that small first-order streams [*Peterson et al.*, 2001] are important locations of nitrogen (N) transport and retention that can strongly affect downstream N exports [*Alexander et al.*, 2000; *Gomez-Velez et al.*, 2015; *Howard-Williams et al.*, 1983; *Kiel and Cardenas*, 2014]. There is widespread evidence that N can be removed from water ways during its downstream transport through watersheds [*Engler and Patrick*, 1974; *Kaushik and Robinson*, 1976]. The fraction of removal of N in streams compared to the overall N budget in watersheds could reach 40% or even more [*Birgand et al.*, 2007]. Nitrogen could be temporarily reduced within the stream water through, for example, assimilation by plant nitrogen uptake [*Howard-Williams et al.*, 1983] and storage of N in the sediment [*Birgand et al.*, 2007; *Svendsen and Kronvang*, 1993]. The broad literature on the removal of N in streams highlighted the critical role of denitrification. Denitrification is considered as the main mechanism that could permanently remove NO_3^- from stream ecosytems. For example, it has been suggested that at least half of the NO_3^- entering river systems appears to be "lost" due to denitrification on its way to the ocean [*Alexander et al.*, 2009; *Galloway et al.*, 2003].

Streams and aquifers are two critical parts of the hydrosphere that are intimately connected through the hyporheic zone (HZ), which is the transition zone between the surface water and subsurface water in fluvial systems. Pore water in subsurface sediment is continuously circulated through and exchanged with the overlying surface water defining HZs. Hyporheic exchange drives advection of solute mass and energy and

exerts a strong influence on the quality of both surface and subsurface waters and on fluvial ecology [*Boano et al*., 2014; *Cardenas*, 2015; *Harvey and Gooseff*, 2015]. A large number of factors influence hyporheic exchange, which have been investigated in previous studies through mathematical models, flume experiments, and field studies. These physical factors include streambed topography, sediment permeability and heterogeneity, large woody debris, and other obstacles in rivers, stream discharge, and stream curvature [*Cardenas*, 2008; *Cardenas et al*., 2004; *Packman and Salehin*, 2003; *Sawyer et al*., 2011].

HZs are recognized as ecotones or perhaps a unique ecosystem providing vital functions [*Boulton et al*., 1998; *Brunke and Gonser*, 1997; *Findlay*, 1995; *Jones and Holmes*, 1996; *Stanford and Ward*, 1988]. The HZ is rich in biologically active sediment, creating a favorable condition for microbially facilitated reactions to occur, including organic carbon oxidation (aerobic respiration), nitrification, and denitrification. A large number of investigations have shown that the HZs serve as the active sites of N biogeochemical dynamics [*Bardini et al*., 2012; *Cirmo and McDonnell*, 1997; *Duff and Triska*, 1990; *Kessler et al*., 2014; *Zarnetske et al*., 2012], determine the amount and fate of N traveling through the streambed sediment, and are thus influencing water quality in the stream channel [*Harvey et al*., 2013; *Bardini et al*., 2012; *Marzadri et al*., 2012; *Zarnetske et al*., 2012]; these have been shown to be important at the river network scale [*Kiel and Cardenas*, 2014; *Gomez-Velez et al*., 2015].

The biogeochemical reactions in the HZ could produce or consume inorganic N (NH_4^+ and NO_3^-) and thus affect stream water quality and ultimately ecosystem health [*Groffman et al*., 2005]. The potential function of the HZ as a source or sink of NO_3^- is primarily controlled by the supply and demand of O_2 because O_2 largely determines the redox conditions which regulate where and when nitrification and denitrification occur [*Zarnetske et al*., 2012]. Denitrification in the HZs has been found to reduce NO_3^- levels in streams and rivers which could decrease or buffer eutrophication [*Clément et al*., 2002; *Martin et al*., 2001; *McClain et al*., 2003] when the HZ provides a NO_3^- sink role. On the other hand, HZs can also be a NO_3^- source when nitrification is dominant over denitrification [*Jones et al*., 1995]. In addition to favorable redox conditions, denitrification is also controlled by the availability of labile carbon [*Jones and Holmes*, 1996; *Zarnetske et al*., 2011a, 2011b], and thus, the C and N cycles in the HZ are intimately coupled.

Most biogeochemical reactions are sensitive to temperature, especially bacterially mediated reactions. Thus, temperature could play an important role in the biogeochemical processes within the HZ. Furthermore, HZs are subject to spatially and temporally varying temperatures. For example, a diel temperature pattern following stream water would penetrate through the sediment-water interface (SWI) and result in a dynamic temperature pattern, which could potentially affect the biogeochemical reactions in the HZ [*Cardenas and Wilson*, 2007b; *Norman and Cardenas*, 2014; *Sawyer et al*., 2012; *Swanson and Cardenas*, 2010]. Since rivers are subject to seasonal temperature changes, so are their HZs. However, there have been few studies focused on coupling and integrating fluid flow, heat transport, and reactive solute transport to understand the complex links and feedbacks between hydrodynamic, biogeochemical, and thermal processes in the HZ. Therefore, an integrated framework is necessary.

The goal of this study is to understand and quantify the effect of temperature on nitrate removal and production efficiency in bed form-induced hyporheic zones. We investigated and analyzed the pertinent coupled processes of fluid flow and temperature-dependent biogeochemical reactions. We used multiphysics numerical models that integrate all the above processes but focus on N biogeochemistry. We take into account four representative reactive compounds pertinent in N cycling: dissolved organic carbon (DOC), dissolved oxygen (DO), nitrate (NO_3^-), and ammonium (NH_4^+). These species are usually used as direct indicators of water quality in field studies, and they have direct influence on many aquatic ecosystems [*Bardini et al*., 2012]. Since the effects of dynamic temperatures are potentially complex, we first study the steady temperature effect. This paper addresses the steady temperature effect on nitrate removal-production efficiency; future work will analyze the effect of diurnal temperature variations.

A series of numerical simulations with different homogeneous temperatures, increasing from 5°C to 35°C in increments of 5°C, were conducted. The models simulated the distributions of chemical species and reaction rates in the HZ. Integration of nitrification, denitrification, and net denitrification rates in the HZ was conducted to further evaluate the overall NO_3^- removal or production efficiency occurring within the HZ. We focused on two stream water quality scenarios, a polluted stream and a pristine stream following *Bardini et al*. [2012]. A sensitivity analysis was performed to gain broader insight.

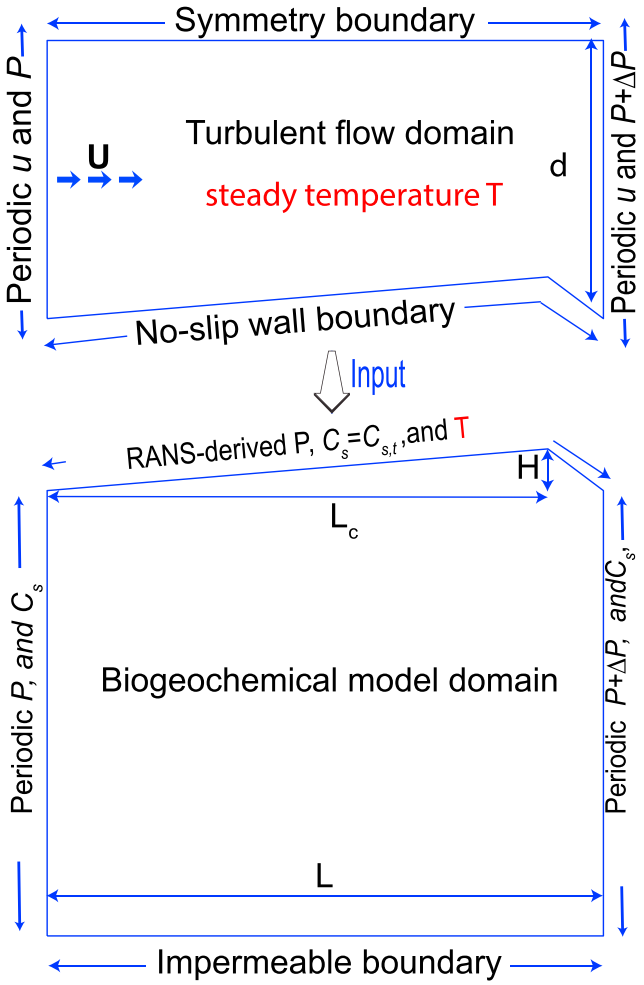

Figure 1. Schematic representation of numerical modeling approach for the physical-biogeochemical processes occurring in a representative bed form-induced hyporheic zone. The streambed length $L = 1$ m, height $H = 0.05$ m, with the crest at $0.9\,L$ ($L_c = 0.9$ m), and the sediment thickness is 0.8 m. (top) The stream flow (water depth $d = 0.5$ m). (bottom) The permeable porous sediment. T is temperature, P is pressure, C is solute concentration, and U is stream velocity.

2. Methodology and Theoretical Background

The modeling scheme follows those presented previously in *Cardenas and Wilson* [2007a, 2007b] and *Bardini et al.* [2012, 2013]; this is conceptually illustrated in Figure 1. Briefly, the method is as follows: (1) turbulent open channel flow was modeled above a dune bed form, (2) the pressure along the SWI from the turbulent flow model was used as a boundary condition for a groundwater flow model, and (3) the groundwater flow field was used to model reactive transport where the reaction kinetics are temperature dependent. For this study, a steady and homogeneous temperature field was assumed.

2.1. Turbulent Flow Modeling for Pressure Distribution Along the Interface

Mean unidirectional turbulent flow in the water column over the bed form was modeled by numerically solving a finite-volume formulation of Reynolds-averaged Navier-Stokes (RANS) equations for an incompressible, homogeneous and isothermal fluid with the k-ω closure scheme [*Wilcox*, 1991]. This approach has been validated showing that the simulated pressure profiles along the SWI agree reasonably well with experimental observations [*Cardenas and Wilson*, 2007a; *Janssen et al.*, 2012]. In this study, we did not actually conduct additional turbulent flow modeling. Instead, we took the result of one model from *Cardenas and Wilson* [2007b]. But for completeness, below we briefly discuss the pertinent model conditions and parameters.

A symmetry boundary condition was used at the top of the RANS domain [*Cardenas and Wilson*, 2007a]. Spatially periodic pressure conditions were prescribed on the lateral boundaries, with a specified pressure drop (ΔP) [*Bardini et al.*, 2012] between the left and right boundaries of the RANS domain which represents the channel slope. The bottom of the domain (the sediment-water interface, SWI) was treated as a no-slip wall boundary condition that neglects the influence of subsurface flow below the RANS domain. We retrieved the time-averaged pressure distribution (considered as the steady state pressure) along the SWI from the RANS simulation. This pressure distribution is further used as a Dirichlet boundary condition for simulating fluid flow through the porous sediment and thus determined the hyporheic exchange across the SWI and flow within the HZ. The RANS model result used here has a water depth of 0.5 m above the trough and a mean flow velocity of 0.4 m/s, leading to a Reynolds number of 20,000 (with the bed form crest height as the characteristic length scale). In all models, the bed form length is $L = 1$ m, and height is $H = 0.05$ m, with the crest at $0.9\,L$.

Table 1. Chemical Reactions Considered in the Simulations

Reaction Type	Reaction
Aerobic respiration	$CH_2O + O_2 \rightarrow CO_2 + H_2O$
Denitrification	$5CH_2O + 4NO_3^- + 4H^+ \rightarrow 5CO_2 + 2N_2 + 7H_2O$
Nitrification	$NH_4^+ + 2O_2 \rightarrow NO_3^- + 2H^+ + H_2O$

2.2. Pore Water Flow Through the Sediment

Two-dimensional porous media flow in the sediment (Figure 1) is solved using the steady state groundwater flow equations (i.e., the continuity equation and Darcy's law) which read as

$$\nabla \cdot q = 0 \tag{1}$$

$$q = -\frac{k_p}{\mu(T)}\nabla P \tag{2}$$

where q is the Darcy flux, k_p is intrinsic permeability, μ is the fluid viscosity depending on T, and P is the pressure.

The top boundary of the porous domain (the SWI) is a Dirichlet boundary defined by the RANS-derived pressure distribution. The lateral boundaries are spatially periodic boundaries with a prescribed pressure drop (ΔP) (Figure 1), which is the same as applied for the RANS domain. This approach results in a continuous pressure distribution across the RANS domain and porous domain [*Cardenas and Wilson*, 2007a]. The bottom of the porous flow domain, which is at a depth of 0.8 m, was assigned as a no-flux boundary. The sediment is assumed to be homogeneous and isotropic with a $k_p = 5 \times 10^{-11}$ m^2 which roughly corresponds to medium to coarse sand.

2.3. Multicomponent Reactive Transport Modeling

Hyporheic flow carries carbon, nutrients, and dissolved oxygen into the sediment that makes microbially facilitated reactions more likely to occur in the biologically active sediments. In particular, we consider four representative reactive compounds: dissolved organic carbon (DOC), dissolved oxygen (DO), nitrate (NO_3^-), and ammonium (NH_4^+). Formaldehyde (CH_2O) is used here to represent complex DOC substrate due to its simple chemical structure following *Bardini et al*. [2012]. We do not consider particulate organic carbon (POC) specifically in this study, since POC particles could affect the permeability of the sediment and distribution of the bacteria community, which may make the system too complex to study. We assume that all the nutrients and carbon in the sediments come from the penetration of stream water in the streambed. The multicomponent reactive transport model explicitly simulates three critical chemical reactions that govern nitrogen biogeochemistry: nitrification (NI), denitrification (DN), and aerobic respiration of dissolved organic matter (AR) (Table 1). All other N transformation processes, such as ammonification, assimilation, and anammox, are neglected in the numerical models.

In this study, the microbial degradation of organic compounds was considered as a primary reaction and serves as the ultimate source of chemical energy [*Hunter et al*., 1998]. For simplicity, first-order degradation kinetics is assumed for the DOC oxidation rate r_{DOC}

$$r_{DOC} = k_{DOC} \cdot [DOC] \tag{3}$$

where k_{DOC} is the first-order reaction rate constant (i.e., the DOC decay constant); brackets correspond to actual activity of DOC concentration, and the activity coefficient is assumed to be 1. The linear kinetics in equation (3) is the simplest way to represent DOC degradation [*Bardini et al*., 2012]. This further implies that the availability of primary organic substrate determines the overall degree of enzymatic activity of the microbial community [*Hunter et al*., 1998]. Aerobic respiration and nitrification are assumed to occur simultaneously, while denitrification only occurs when the oxygen concentration drops under a limiting value.

We assume that the electrons released by DOC degradation are transferred to the potential terminal electron acceptors, such as O_2 and NO_3^-, which are used by microorganisms sequentially. Then the reduction rate of $r_{red,i}$ of the ith electron acceptor ($i = 1$ for O_2 and $i = 2$ for NO_3^-) can be estimated by

$$r_{red,i} = f_i \cdot r_{DOC} \cdot \beta_i \quad (i = 1, 2) \tag{4}$$

where f_i is the fraction of electrons consumed by the ith reduction half-reaction and β_i is the ratio between the moles of transferred electrons per mole of oxidized DOC and the moles of electrons per mole of reduced

Table 2. In-Stream and Hyporheic Inflow Boundary Concentrations of Solutes

Case	[DOC] (mg/L)	[O_2] (mg/L)	[NO_3^-] (mg/L)	[NH_4^+] (mg/L)	[NO_3^-]/[NH_4^+]
Polluted stream	150	10	8	5	1.6
Pristine stream	50	10	1	0.05	20

compound in the ith reaction. The fraction f_i is defined with a simplified Monod formulation for the utilization of the terminal electron acceptors [*Bardini et al.*, 2012; *Hunter et al.*, 1998] following

$$f_i = \left(1 - \sum_{n=0}^{i-1} f_n\right) \cdot \alpha_i \tag{5}$$

with $f_0 = 0$ and

$$\alpha_i = \begin{cases} \dfrac{C_i}{C_{i,\mathrm{lim}}} & \text{if } C_i < C_{i,\mathrm{lim}} \\ 1 & \text{if } C_i \geq C_{i,\mathrm{lim}} \end{cases} \tag{6}$$

where C_i and $C_{i,\mathrm{lim}}$ are the molar concentration and the molar limiting concentration of the ith reaction electron acceptor, respectively. α_i is a dimensionless parameter that assumes that each electron acceptor has a limiting concentration ($C_{i,\mathrm{lim}}$). When the concentration of this electron acceptor (C_i) exceeds its threshold, the corresponding half-reaction rate is independent of C_i. Otherwise, the rate is proportional to C_i (i.e., first-order dependence). According to the preferential order of utilization of the electron acceptors, f_1 and f_2 correspond to O_2 and NO_3^-, respectively.

Nitrification is described by conventional second-order bimolecular reaction kinetics

$$r_{\mathrm{NH_4^+}} = k_{\mathrm{NH_4^+}} \cdot \left[\mathrm{NH_4^+}\right] \cdot \left[\mathrm{O_2}\right] \tag{7}$$

where $k_{\mathrm{NH_4^+}}$ is the second-order nitrification molar rate coefficient; brackets correspond to the activity of species, and the activity coefficient is assumed to be 1.

Some species play dual roles in reactions, taking part not only as reactants but also as products. We define the net reaction rates of those four representative compounds from equations (3)–(7) as follows:

$$R_{\mathrm{DOC}} = -r_{\mathrm{DOC}} \tag{8a}$$

$$R_{\mathrm{O_2}} = -r_{\mathrm{red},1} - 2r_{\mathrm{NH_4^+}} \tag{8b}$$

$$R_{\mathrm{NO_3^-}} = -r_{\mathrm{red},2} + r_{\mathrm{NH_4^+}} \tag{8c}$$

$$R_{\mathrm{NH_4^+}} = -r_{\mathrm{NH_4^+}} \tag{8d}$$

The negative sign indicates that the reactant is consumed and vice versa.

The steady state reactive solute transport through the sediment is described by

$$\nabla \cdot \left(-\theta D \nabla C_j + q \cdot C_j\right) = \theta R_j \quad \left(\mathrm{j} = \mathrm{DOC},\ \mathrm{O_2},\ \mathrm{NO_3^-},\ \mathrm{NH_4^+}\right) \tag{9}$$

where θ is the sediment porosity, R_j (sink/source term) is the net reaction rate of the compound j, D is the hydrodynamic dispersion tensor and C_j is the molar concentration of the species j, and q is the specific discharge as defined in equation (1). The top boundary of the sediment (the SWI) for equation (9) is set as an open boundary. The top boundary is divided into two zones; downwelling parts are treated as a Dirichlet condition with the constant solute concentrations in the stream ($C_{s,t} = C_{s,0}$); upwelling parts are assigned as advective boundaries with no dispersion (zero gradient). The lateral boundaries of the sediment domain are set as periodic boundaries ($C_{s,l} = C_{s,r}$). The bottom is set as no-flow boundary.

The D tensor is calculated following

$$\theta D_{ij} = \alpha_T |q| \delta_{ij} + (\alpha_L - \alpha_T) \cdot q_i q_j / |q| + \theta \cdot \tau D_m \delta_{ij} \quad (i,\ j = 1, 2) \tag{10}$$

where i, $j = 1, 2$; α_L and α_T are transverse and longitudinal dispersivities; τ is the tortuosity factor; δ_{ij} is the Kronecker delta function; and D_m is the molecular diffusion coefficient in porous media. α_L is set to be 3 cm (dozens of grain diameters for sand), and α_T is considered to be $\alpha_L/10$.

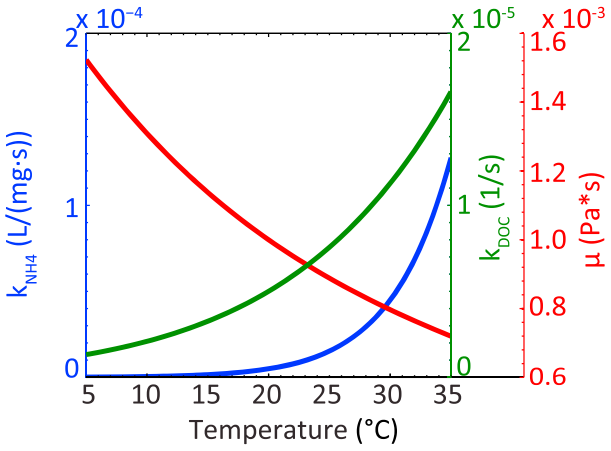

Figure 2. Temperature-dependent parameters: (1) Arrhenius relationship between reaction rate constant of respiration (k_{DOC}) and nitrification (k_{NH4}) and temperature; (2) viscosity (μ) decreases with temperature.

Here we assume that the stream water is well mixed such that the concentration of four species at the top boundary of the sediment is constant. To study the effect of temperature on the nutrient cycling on the HZ, we employed two cases with different in-stream species concentrations following *Bardini et al.* [2012]. The concentrations of the four components are listed in Table 2.

2.4. Temperature-Dependent Kinetics and Hydraulic Parameters

The influence of temperature on biochemical reaction kinetics has been proposed to follow the Arrhenius law [*Dawson and Murphy*, 1972] (see Figure 2)

$$k(T) = Ae^{-E/RT} \tag{11}$$

where $k(T)$ is the reaction rate constant at some temperature T, A is the pre-exponential factor, E is the activation energy of the reaction, and R is the ideal gas constant. For many biochemical reactions, within the appropriate temperature range, the reaction rates could double with a 10°C temperature increase [*Veraart et al.*, 2011]. The Arrhenius equation can be modified to consider temperature changes, resulting in

$$k(T_1) = k(T_2)e^{-\frac{E}{R}\left(\frac{1}{T_1}-\frac{1}{T_2}\right)} \tag{12}$$

From equations (11) and (12), the reaction rate constant at any given temperature can be determined. In this study, we assume that aerobic respiration and nitrification follow an Arrhenius relationship between 5°C and 35°C. Activation energies for aerobic respiration (E_1) and nitrification (E_2) in this study are 60 kJ/mol [*Thamdrup et al.*, 1998; *Yvon-Durocher et al.*, 2012] and 162 kJ/mol [*Sheibley et al.*, 2003], respectively (Table 3).

Additionally, the density (ρ) and viscosity (μ) of water are temperature dependent. Both ρ and μ decrease with increasing temperature, but the influence of temperature on ρ can typically be ignored for the temperature range we considered in this study (5°C to 35°C which translates to a 0.6% decrease in ρ), especially compared to the influence on dynamic viscosity. Since $K_h = k_p\rho g/\mu$, where K_h is the hydraulic conductivity, k_p is the intrinsic permeability, g is the acceleration of gravity, temperature variation affects pore water flow via an effect on K_h. For example, because of decreasing μ with increasing T, the value of K_h doubles when the

Table 3. Summary of Input Parameters for the Reactive Transport Models

Symbol	Unit	Value	Description
D_m	m^2/s	1×10^{-10}	Molecular diffusion coefficient
θ	-	0.4	Porosity
τ	-	$\theta^{1/3}$	Tortuosity
β_1	-	1	Ratio of transferred electrons for O_2
β_2	-	0.8	Ratio of transferred electrons for NO_3^-
$[O_2]_{lim}$	mg/L	1	Oxygen limiting concentration
$[NO_3^-]_{lim}$	mg/L	0.5	Nitrate limiting concentration
k_{NH4+}	L/(mg s)	5×10^{-6}	Second-order nitrification molar rate coefficient at temperature 20°C
k_{DOC}	1/s	5×10^{-6}	DOC decay constant at temperature 20°C
R	J/(K mol)	8.31	Gas constant
E_1	kJ/mol	60	Activation energy for aerobic respiration
E_2	kJ/mol	162	Activation energy for nitrification

temperature is increased from 0°C to 25°C [*Birgand et al.*, 2007]. The viscosity dependence on temperature follows a polynomial function [*Cardenas and Wilson*, 2007b; *Schmidt*, 1979]

$$\mu(T) = a - bT + cT^2 - \mathrm{d}T^3 + eT^4 \tag{13}$$

The coefficients above are $a = 0.00179$, $b = 5.942 \times 10^{-5}$, $c = 1.286 \times 10^{-6}$, $d = 1.623 \times 10^{-8}$, and $e = 8.665 \times 10^{-11}$.

2.5. Numerical Modeling Implementation

The above conceptual model with hydrodynamic and chemical processes is implemented in the generic finite-element modeling software COMSOL Multiphysics. The sediment domain is discretized into ~200,000 triangular elements. To capture the physical and chemical processes occurring at the SWI, we used a refined mesh (~0.005 mm spacing) close to the top boundaries and relatively much coarser elements (~1 mm) within the domain. Additionally, we utilize the boundary layer mesh functionality in COMSOL to further ensure the accuracy of results from the boundary and moving away from it. The numerical results have been tested to be insensitive to the mesh size.

We implemented a parametric modeling approach in COMSOL with increasing temperature from 5°C to 35°C. The implementation of numerical models is also carried out with two cases that represent different stream water qualities (Table 2). The values of all model input parameters are presented in Table 3.

2.6. Definition of N Transformation Reaction Rates

The spatially averaged reaction rates are calculated by integrating the distributed reaction rates over the whole sediment domain and then dividing by the area of the HZ

$$\overline{r_{\mathrm{NI}}} = \frac{1}{A}\int \theta \cdot \mathrm{r}_{\mathrm{NH_4^+}} \cdot \mathrm{d}A \tag{14a}$$

$$\overline{r_{\mathrm{DN}}} = \frac{1}{A}\int \theta \cdot r_{\mathrm{red},2} \cdot \mathrm{d}A \tag{14b}$$

$$\overline{r_{\mathrm{netDN}}} = \frac{1}{A}\int \theta \cdot R_{\mathrm{NO_3^-}} \cdot \mathrm{d}A \tag{14c}$$

Negative net denitrification values ($\overline{r_{\mathrm{netDN}}}$) indicate that the amount of nitrate consumption through denitrification is greater than the amount of nitrate production from nitrification, and vice versa.

3. Results

3.1. Temperature Effect on the Flow Field and Interfacial Fluxes

The hyporheic flow fields at different temperatures are nearly the same (Figures 3 and 4), which shows that temperature hardly has an effect on the flow kinematics. Since the effect of temperature on fluid flow is through temperature-dependent viscosity (i.e., equation (13)) and therefore hydraulic conductivity, as a result, the calculated interfacial flux over the SWI changes from from 9.4×10^{-7} m^2/s at $T = 5$°C to 2.0×10^{-6} m^2/s at $T = 35$°C (Table 4). Although temperature has a measurable effect on the interfacial fluid flux, it expectedly only affects the velocity magnitude and does not alter the general flow pattern (Figures 3 and 4). However, temperature would affect the nutrient cycling in hyporheic zones through the supply rate of solutes, i.e., it affects the reaction rates due to more availability of reactants because of increased hyporheic advection.

To analyze the effects of temperature on the nutrient supply rate, we calculated the total interfacial flux of nitrate into ($\left[\mathrm{NO_3^-}\right]_{\mathrm{in}}$) and out of ($\left[\mathrm{NO_3^-}\right]_{\mathrm{out}}$) the HZ. For the polluted stream case, $\left[\mathrm{NO_3^-}\right]_{\mathrm{in}}$ increases until it peaks at 25°C then decreases with even higher temperature (Table 4). The temperature effect on $\left[\mathrm{NO_3^-}\right]_{\mathrm{in}}$ is less than 1 order of magnitude variation from 5°C to 35°C (Table 4). $\left[\mathrm{NO_3^-}\right]_{\mathrm{out}}$ increases monotonically with temperature. For the pristine stream case, both $\left[\mathrm{NO_3^-}\right]_{\mathrm{in}}$ and $\left[\mathrm{NO_3^-}\right]_{\mathrm{out}}$ always increase with increasing temperature (Table 5). The main difference between these two cases is the relative abundance of ammonium and nitrate; [NO_3^-]/[NH_4^+] of the polluted stream case is 1.6, while [NO_3^-]/[NH_4^+] of the pristine stream case is 20 (Table 2).

3.2. Temperature Effect on Nutrient Distribution

The resultant spatial distributions of the four N species at steady state are shown in Figure 3 (polluted stream case) and Figure 4 (pristine stream case). DOC, DO, and NH_4^+ concentrations, which are set by the boundary

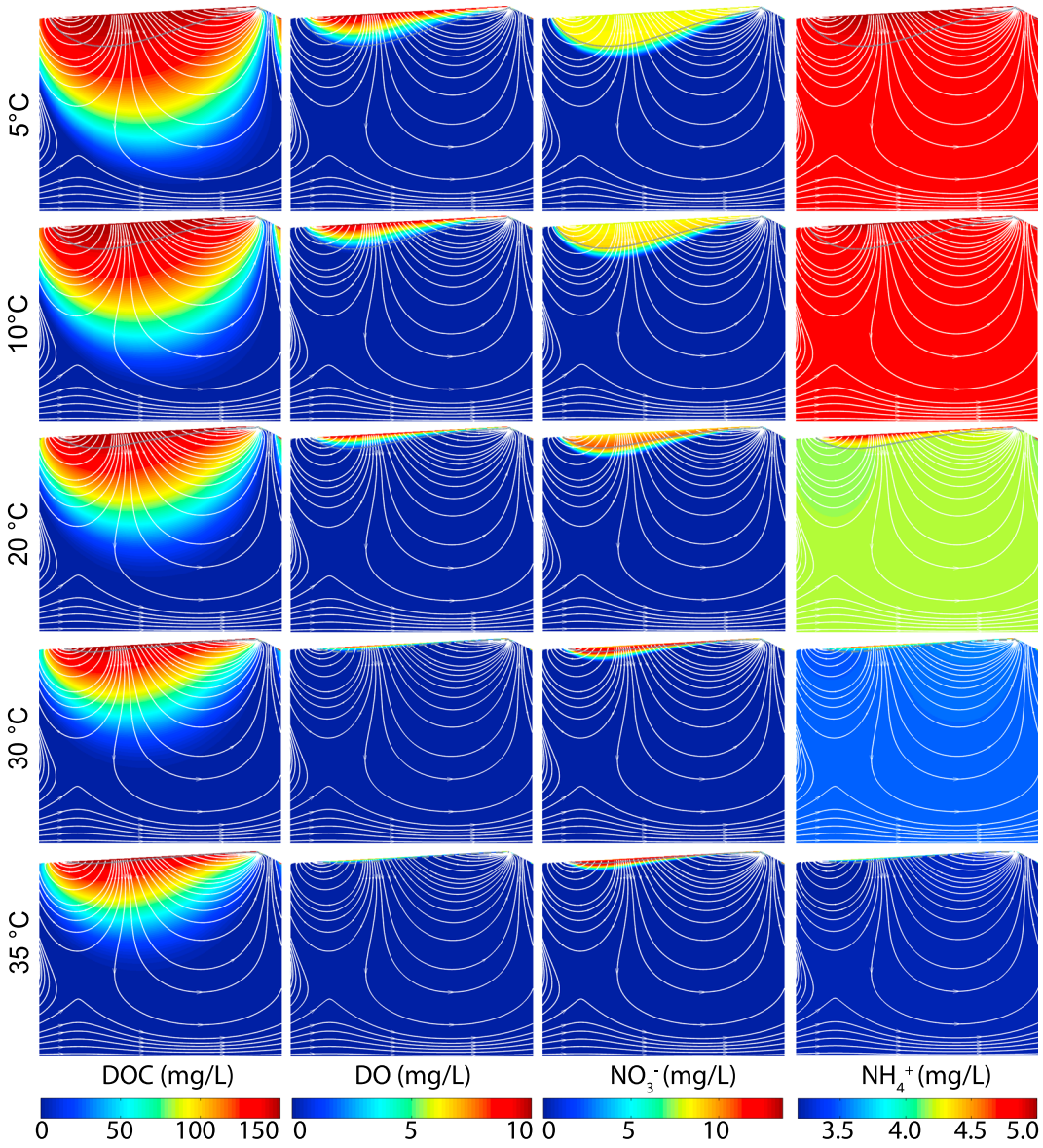

Figure 3. Solute-spatial distribution with varying temperatures for the polluted stream case. Channel flow is from left to right. White lines with arrows indicate streamlines. Gray dotted lines indicate the oxic-anoxic boundary. The domain is 1 m wide.

condition at the SWI, decrease with depth for both cases. The solute fronts are similar in shape but different in size, i.e., they all have a parabolic or semicircular shape and front, and the deepest portion is located at the divide of two counter-flowing advective flow cells (i.e., near the stagnation point). The smooth solute concentration fronts imply that dispersion plays an important role for delivering and distributing solutes into the HZ.

NO_3^- displays a different behavior relative to the other three species, with the maximum concentration just above the oxic-anoxic zone boundary (Figures 3 and 4). This is because nitrification occurs in the oxic zone with the nitrate produced advected downward further along the hyporheic flow path, whereas the removal of nitrate through denitrification begins only when oxygen is depleted or drops below the limiting concentration. In this study, the DO limiting concentration of 1 mg/L is defined as the oxic-anoxic boundary. In short, nitrification prevails above the oxic-anoxic boundary occurring in the shallow sediment, while denitrification dominates below the oxic-anoxic boundary in the deep sediment. In addition, the NO_3^- front is steeper than the DOC, DO, and NH_4^+ concentration fronts. This is because additional nitrate is supplied from nitrification, which is then removed by denitrification very quickly, thus spatially constraining the denitrification zone.

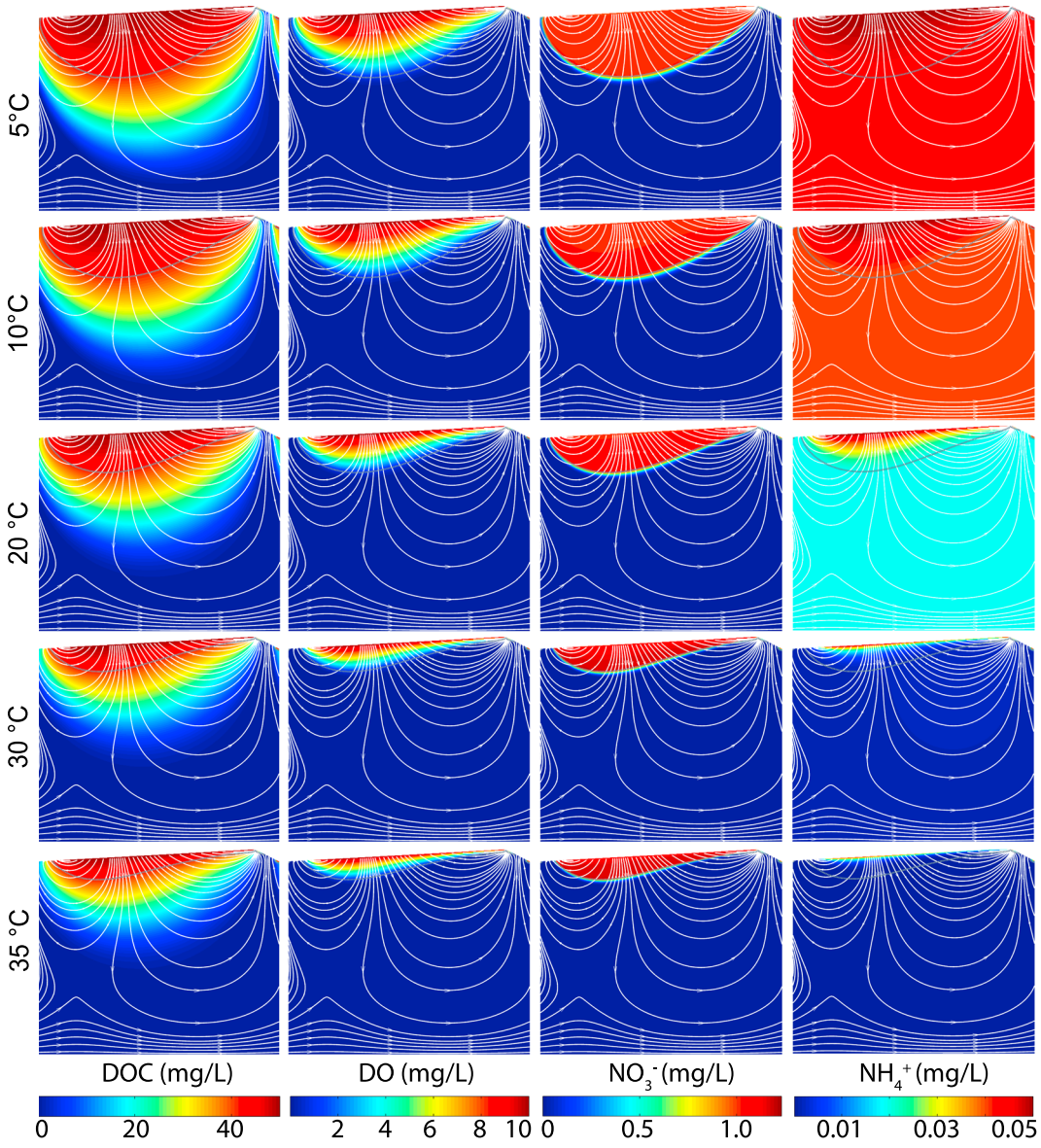

Figure 4. Solute-spatial distribution with varying temperatures for the pristine stream case. Channel flow is from left to right. White lines with arrows indicate streamlines. Gray dotted lines indicate the oxic-anoxic boundary. The domain is 1 m wide.

Table 4. Summary of Simulation Results for the Polluted Stream Case

T °C	HZ Flux (m^2/s)	$[NO_3]_{in}$ mg/(m s)	$[NO_3]_{out}$ mg/(m s)	$[NO_3]_{advin}$ mg/(m s)	$[NO_3]_{dspout}$ mg/(m s)	$\overline{r_{NI}}$ mg/(m^3 s)	$\overline{r_{DN}}$ mg/(m^3 s)	$\overline{r_{netDN}}$ mg/(m^3 s)	N_A mg/(m s)	N_{RE}
5	9.4×10^{-7}	-7.6×10^{-3}	4.4×10^{-3}	-7.6×10^{-3}	4.4×10^{-3}	3.5×10^{-4}	4.2×10^{-3}	-3.9×10^{-3}	-3.2×10^{-3}	42.4%
10	1.1×10^{-6}	-8.8×10^{-3}	4.8×10^{-3}	-8.8×10^{-3}	4.8×10^{-3}	8.6×10^{-4}	5.7×10^{-3}	-4.8×10^{-3}	-4.0×10^{-3}	45.8%
15	1.3×10^{-6}	-1.0×10^{-2}	5.2×10^{-3}	-1.0×10^{-2}	5.2×10^{-3}	1.9×10^{-3}	7.7×10^{-3}	-5.8×10^{-3}	-4.9×10^{-3}	48.5%
20	1.4×10^{-6}	-1.1×10^{-2}	5.6×10^{-3}	-1.1×10^{-2}	5.6×10^{-3}	3.7×10^{-3}	1.0×10^{-2}	-6.6×10^{-3}	-5.5×10^{-3}	49.9%
25	1.6×10^{-6}	-1.2×10^{-2}	6.0×10^{-3}	-1.2×10^{-2}	6.0×10^{-3}	6.8×10^{-3}	1.4×10^{-2}	-6.7×10^{-3}	-5.6×10^{-3}	48.5%
30	1.8×10^{-6}	-1.1×10^{-2}	6.6×10^{-3}	-1.1×10^{-2}	6.6×10^{-3}	1.2×10^{-2}	1.7×10^{-2}	-5.3×10^{-3}	-4.5×10^{-3}	40.5%
35	2.0×10^{-6}	-8.4×10^{-3}	7.5×10^{-3}	-8.4×10^{-3}	7.5×10^{-3}	2.0×10^{-2}	2.1×10^{-2}	-1.1×10^{-3}	-9.0×10^{-4}	10.7%

Table 5. Summary of Simulation Results for the Pristine Stream Case

T (°C)	HZ flux (m^2/s)	$[NO_3]_{in}$ mg/(m s)	$[NO_3]_{out}$ mg/(m s)	$[NO_3]_{advin}$ mg/(m s)	$[NO_3]_{dspout}$ mg/(m s)	$\overline{r_{NI}}$ mg/(m^3 s)	$\overline{r_{DN}}$ mg/(m^3 s)	$\overline{r_{netDN}}$ mg/(m^3 s)	N_A mg/(m s)	N_{RE}
5	9.4×10^{-7}	-9.5×10^{-4}	6.9×10^{-4}	-9.5×10^{-4}	6.9×10^{-4}	9.4×10^{-6}	3.3×10^{-4}	-3.2×10^{-4}	-2.7×10^{-4}	28.3%
10	1.1×10^{-6}	-1.1×10^{-3}	7.4×10^{-4}	-1.1×10^{-3}	7.4×10^{-4}	2.4×10^{-5}	4.6×10^{-4}	-4.4×10^{-4}	-3.7×10^{-4}	33.1%
15	1.3×10^{-6}	-1.3×10^{-3}	8.0×10^{-4}	-1.3×10^{-3}	8.0×10^{-4}	5.6×10^{-5}	6.2×10^{-4}	-5.7×10^{-4}	-4.8×10^{-4}	37.3%
20	1.4×10^{-6}	-1.4×10^{-3}	8.6×10^{-4}	-1.4×10^{-3}	8.6×10^{-4}	1.1×10^{-4}	8.2×10^{-4}	-7.1×10^{-4}	-5.9×10^{-4}	40.9%
25	1.6×10^{-6}	-1.6×10^{-3}	9.1×10^{-4}	-1.6×10^{-3}	9.1×10^{-4}	1.9×10^{-4}	1.0×10^{-3}	-8.5×10^{-4}	-7.1×10^{-4}	44.0%
30	1.8×10^{-6}	-1.8×10^{-3}	9.5×10^{-4}	-1.8×10^{-3}	9.5×10^{-4}	2.8×10^{-4}	1.3×10^{-3}	-9.9×10^{-4}	-8.3×10^{-4}	46.4%
35	2.0×10^{-6}	-1.9×10^{-3}	1.0×10^{-3}	-1.9×10^{-3}	1.0×10^{-3}	4.0×10^{-4}	1.5×10^{-3}	-1.1×10^{-3}	-9.2×10^{-4}	48.0%

Additionally, the penetration depth of NO_3^- is barely deeper than the oxygen penetration depth at the same temperature. The main difference between the two water quality scenarios is that the concentration front of NO_3^- in the pristine stream case (Figure 4) is sharper and penetrates deeper than that of the polluted stream case (Figure 3). This shows that below the oxic zone, NO_3^- is quickly consumed. But in the pristine stream case, oxygen is consumed slowly thus allowing for deeper penetration of NO_3^-. For the polluted stream case, due to the high concentration of DOC and NH_4^+, oxygen is quickly consumed, and thus, the NO_3^- does not make it to greater depths since denitrification occurs at shallower depths.

The DOC concentration in both water quality scenarios is relatively high; DOC is not the limiting reactant. Thus, aerobic respiration would primarily be limited by the oxygen supply rate. The availability of DOC would therefore have minimal effect on the fate of oxygen and consequently is less relevant to the denitrification

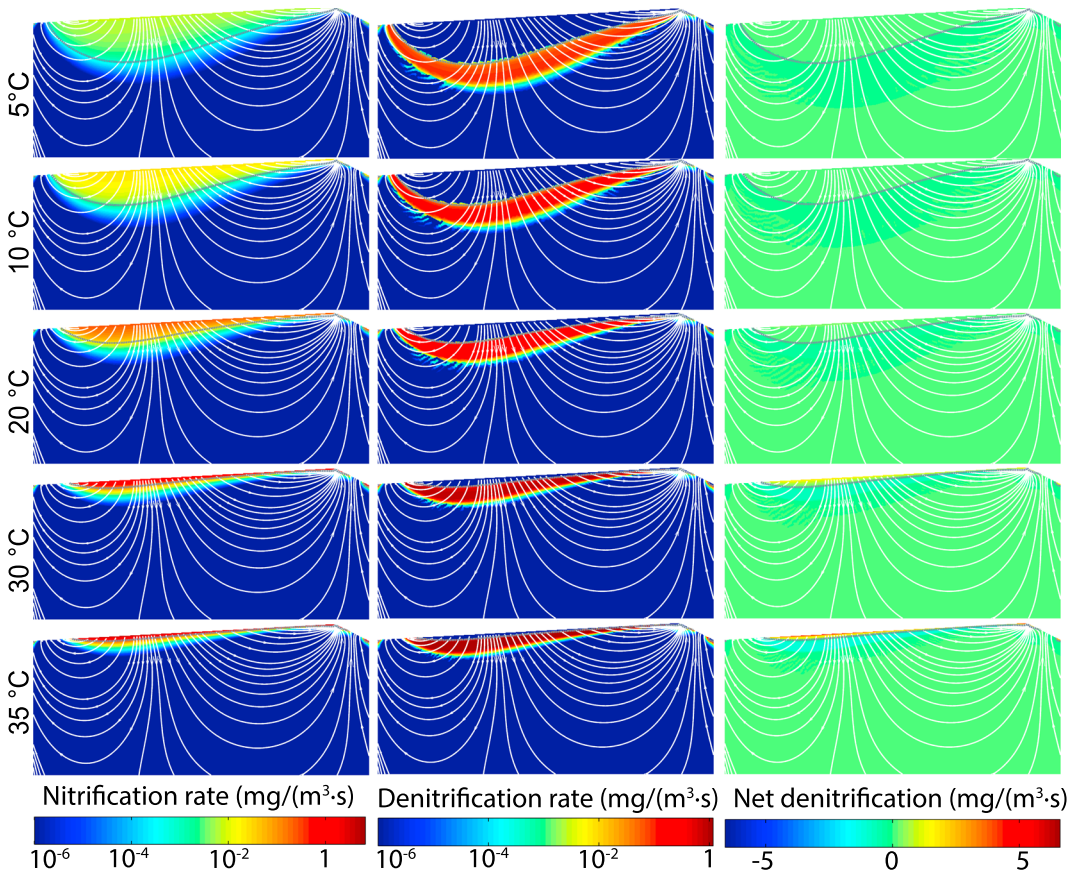

Figure 5. Distribution of nitrification, denitrification, and net denitrification rates with varying temperatures for the polluted stream case. Channel flow is from left to right. White lines with arrows indicate streamlines. Gray dotted lines indicate the oxic-anoxic boundary. The domain is 1 m wide.

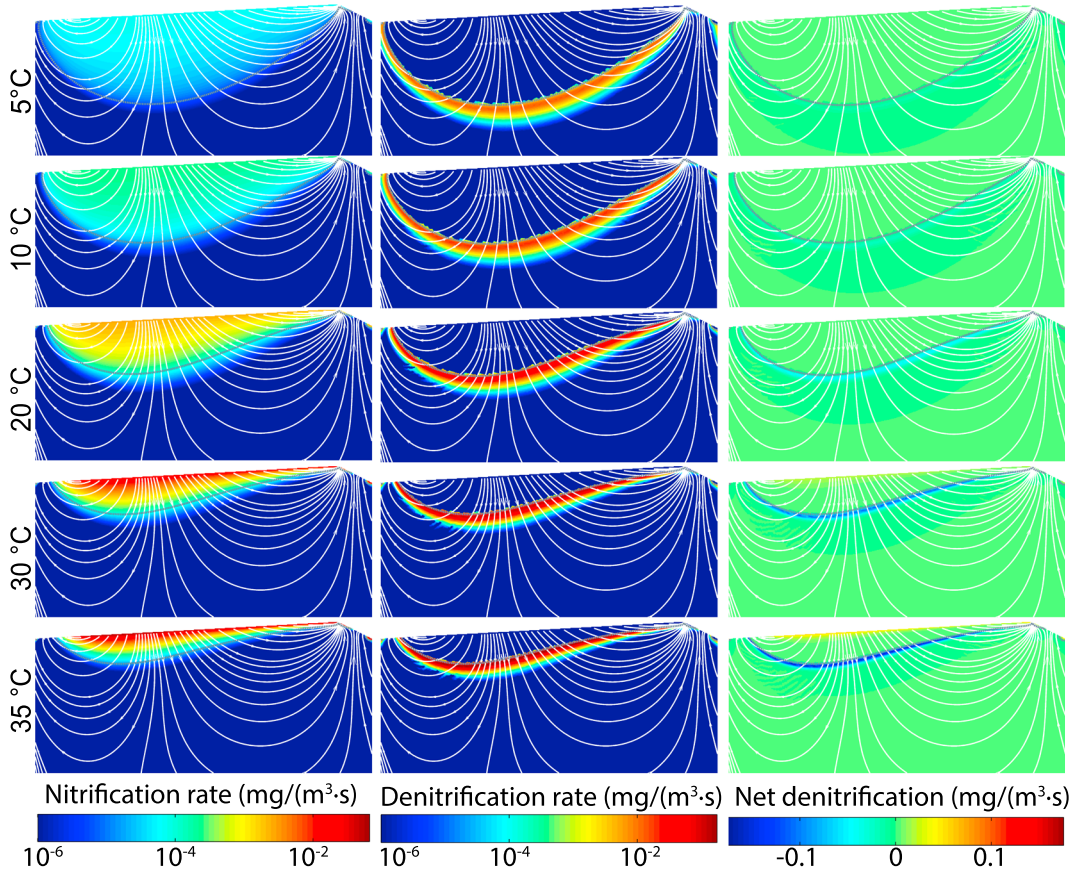

Figure 6. Distribution of nitrification, denitrification, and net denitrification rates with varying temperatures for the pristine stream case. Channel flow is from left to right. White lines with arrows indicate streamlines. Gray dotted gray lines indicate the oxic-anoxic boundary. The domain is 1 m wide.

rates in our study. For the same temperature, as expected, the penetration depth of DOC is deeper than those of DO and NO_3^- at steady state (Figures 3 and 4). Due to the high DOC concentration, DO always becomes depleted at a certain depth due to respiration and nitrification. Any ammonium that is not nitrified in the oxic zone is simply transported further along the hyporheic flow paths (Figures 3 and 4).

The fate of the different solutes is affected differently by temperature. In general, the penetration depths of all solutes considered decreased with increasing temperature (Figures 3 and 4) due to the consumptive biogeochemical reaction rates increasing with temperature. In particular, the oxic zone became shallower and narrower as temperature increased. The oxic-anoxic boundary moved up from ~8 cm depth at 5°C to ~1 cm at 35°C for the polluted stream case (Figure 3) and from ~21 cm at 5°C to ~ 5 cm at 35°C for the pristine stream case (Figure 4). This is a clear consequence of aerobic respiration and nitrification rates increasing with temperature (Figure 2). The reactions rates are analyzed in more detail below.

3.3. Temperature Effect on Reaction Rates

The spatial patterns of nitrification, denitrification, and net denitrification rates for the polluted and pristine cases (Figures 5 and 6) further illustrate that nitrification prevails in the oxic zone and that denitrification dominates in the anoxic zone. The nitrification rate has its maximum value near the SWI due to the abundance of NH_4^+ and O_2, but it declined with depth due to the depletive consumption of both reactants. Moreover, the denitrification rate peaked right below the oxic-anoxic boundary and dropped sharply with depth afterward, thus leading to a very narrow but pronounced denitrification zone. Both nitrification and denitrification reaction areas decrease by about 5–10 times as the temperature increases from 5°C to 35°C (Figures 5 and 6).

Both nitrification and denitrification processes are sensitive to temperature variation (Figure 5). For the polluted stream case, the maximum nitrification rate increased from 2.7×10^{-2} mg/(m^3 s) at 5°C to

2.7×10^{1} mg/(m^3 s) at 35°C, roughly a thousandfold increase. Moreover, the maximum denitrification rate increased from 3.0×10^{-1} mg/(m^3 s) at 5°C to 3.9 mg/(m^3 s) at 35°C (Figure 5), which is a tenfold increase. However, the overall denitrification zone became shallower from a depth of ~8 cm at 5°C to ~1 cm at 35°C; the nitrification and oxic zones moved up correspondingly (Figure 5). For the pristine stream case, the maximum nitrification rate increased from 2.7×10^{-4} mg/(m^3 s) at 5°C to 2.8×10^{-1} mg/(m^3 s) at 35°C; this is still around a thousandfold increase, but the rates were relatively and generally much lower than the polluted case. The maximum denitrification rate increased from 4.8×10^{-2} mg/(m^3 s) at 5°C to 5.8×10^{-1} mg/(m^3 s) at 35°C (Figure 6), which is once again roughly a tenfold increase. Similar to the polluted stream case, the denitrification zone became shallower from a depth of ~21 cm at 5°C to ~5 cm at 35°C. The nitrification and oxic zones moved upward correspondingly.

To further analyze the overall temperature effect on the key chemical reactions over the whole HZ, we evaluated the spatially averaged value for nitrification rate $\overline{r_{\mathrm{NI}}}$, denitrification rate $\overline{r_{\mathrm{DN}}}$, and net denitrification rate $\overline{r_{\mathrm{netDN}}}$, as defined in equations 14a, 14b, 14c. The polluted stream case $\overline{r_{\mathrm{NI}}}$ increased from 3.5×10^{-4} mg/(m^3 s) at 5°C to 2.0×10^{-2} mg/(m^3 s) at 35°C; $\overline{r_{\mathrm{DN}}}$ increased from 4.2×10^{-3} mg/(m^3 s) at 5°C to 2.1×10^{-2} mg/(m^3 s) at 35°C; $\overline{r_{\mathrm{netDN}}}$ became more negative from -3.9×10^{-3} mg/(m^3 s) at 5°C to -6.6×10^{-3} mg/(m^3 s) at 25°C and then increased to -1.1×10^{-3} mg/(m^3 s) at 35°C (Table 4). A negative value for $\overline{r_{\mathrm{netDN}}}$ means denitrification is dominant in the HZ; the HZ consumes nitrate and is a nitrate sink. Additionally, for the pristine stream case, $\overline{r_{\mathrm{NI}}}$ increased from 9.4×10^{-6} mg/(m^3 s) at 5°C to 4.0×10^{-4} mg/(m^3 s) at 35°C; $\overline{r_{\mathrm{DN}}}$ increased from 3.3×10^{-4} mg/(m^3 s) at 5°C to 1.5×10^{-3} mg/(m^3 s) at 35°C; $\overline{r_{\mathrm{netDN}}}$ became more negative from -3.2×10^{-4} mg/(m^3 s) at 5°C to -1.1×10^{-3} mg/(m^3 s) at 35°C (Table 5). In summary, the temperature effect on nitrification is nearly a 2 order of magnitude increase and on denitrification is a 1 order of magnitude increase from 5°C to 35°C (Tables 4 and 5).

There are numerous confounding and interacting factors that ultimately combine to lead to the final temperature dependence of reaction rates. First, equations (3) and (7) dictate that the resulting reaction rate is a function of both the rate constants (which are temperature dependent) and the concentration of reactants. Following the Arrhenius equation (equation (11)), K_{NH4} increases from 1.38×10^{-7} L/(mg s) at 5°C to 1.27×10^{-4} L/(mg s) at 35°C, roughly a thousandfold increase (Figure 2). Likewise, k_{DOC} increases from 1.32×10^{-6} (1/s) at 5°C to 1.66×10^{-5} (1/s) at 35°C, nearly a tenfold increase (Figure 2). As mentioned above and as follows, temperature also has an effect on the interfacial fluid flux which roughly doubles from 9.4×10^{-7} m^2/s at $T = 5$°C to 2.0×10^{-6} m^2/s at $T = 35$°C (Table 4). Additionally, spatially averaged reaction rates are obviously affected by the spatial extent over which the reactions take place. We found that reaction area decreases with increasing temperature, with nearly a 10–20 times reduction for nitrification area and ~2 times reduction for denitrification area (Figures 5 and 6). Furthermore and finally, nitrification, denitrification, and aerobic respiration occur simultaneously. One species (i.e., NO_3^-) can be both a reactant and product in different reactions. This further complicates the sensitivities of reaction rates to temperature. As to the relative importance of these factors on reaction rates, the temperature effect on the rate constant can be considered as the dominant factor. However, the temperature effect on maximum reaction rates and spatially averaged reaction rates cannot be anticipated and exactly predicted by the Arrhenius equation.

4. Discussion

4.1. Temperature Effect on Hyporheic NO_3^- Removal Ability and Efficiency

We employed NO_3^- removal or production ability (N_A) and its associated efficiency (N_{RE}) as two metrics to evaluate the HZ functionality as a NO_3^- source or sink and to estimate the HZ efficiency in N transformation, respectively. The net denitrification rate over the HZ, N_A, which also integrates the coupled nitrification-denitrification process on the mass change rate of nitrate, is defined as

$$N_A = \int R_{\mathrm{NO_3^-}} \cdot \mathrm{d}A \tag{15}$$

where $N_A < 0$ implies that the HZ is a net denitrifying system, in which denitrification dominates over nitrification, and thus, the HZ serves as a nitrate sink. When $N_A > 0$, it implies that the HZ is a net nitrifying system, where nitrification dominates over denitrification, and thus, the HZ is a nitrate source. The magnitude of N_A indicates the extent of nitrate removal or production in the HZ.

Both nitrification and denitrification reaction rates increase as temperature increases from 5°C to 35°C, while nitrification reaction area decreases 10–20 times, and denitrification reaction area decreases ~2 times (Figures 5 and 6). Spatially averaged nitrification rate ($\overline{r_{NI}}$) increases nearly a hundred times, while denitrification ($\overline{r_{DN}}$) increases less than 10 times, and net denitrification ($\overline{r_{netDN}}$) showed a tenfold change from 5°C to 35°C (Table 4 and 5). If reaction area was kept constant, $\overline{r_{NI}}$ would have to increase nearly a thousand times, $\overline{r_{NI}}$ would be larger than $\overline{r_{DN}}$, and nitrification would dominate over denitrification at higher temperature. N_A would have to change from negative values (nitrate sink) at low temperature to positive at high temperature (nitrate source). This implies that reaction area also has a compensating effect on the spatially averaged reaction rates and N_A.

N_{RE} is a dimensionless number that compares reaction and supply rates [*Zarnetske et al.*, 2012] and is defined as

$$N_{RE} = \begin{cases} \dfrac{|N_A|}{\left|\left[NO_3^-\right]_{in}\right|} & N_A < 0 \\ \dfrac{-|N_A|}{\left|\left[NO_3^-\right]_{in}\right| + |N_A|} & N_A \geq 0 \end{cases} \tag{16}$$

where $\left[NO_3^-\right]_{in}$ is the total influx of NO_3^- into the HZ. Similar to N_A, N_{RE} is a useful dimensionless metric describing whether the HZ is a nitrate source or sink. The range of N_{RE} is between 0 and 1 if the HZ is a nitrate sink with larger values indicating higher removal efficiency, where denitrification is dominant over nitrification. If the HZ is a nitrate source, N_{RE} ranges from -1 to 0 with more negative values signifying that more nitrate is being produced in the HZ rather than being carried into the HZ across the SWI.

For the polluted stream case, the N_A increased with temperature until it peaked at 25°C and then decreased with increasing temperature; the N_{RE} increased from 42.4% at 5°C to 49.9% (maximum) at 20°C then decreased to 10.7% at 35°C (Table 4). However, for the pristine stream case, both N_A and N_{RE} increased with increasing temperature, and the N_{RE} changed from 28.3% at 5°C to 48.0% at 35°C (Table 5). The temperature effects on N_A and N_{RE} are different.

To further explain the different trends in N_A and N_{RE} with temperature, we scrutinized the terms in equation (15). For $\left[NO_3^-\right]_{in}$, we expect that it should increase as the temperature increases because the interfacial flux across the SWI increases when the temperature goes up (Tables 4 and 5). However, the $\left[NO_3^-\right]_{in}$ increases at first, reaches its maximum value around 25°C, and then eventually decreases on with even higher temperatures for the polluted stream case (Table 4). This is because the nitrification rate increases with temperature at the oxic zone (i.e., near the top of sediment), resulting in the production of a relatively large amount of NO_3^- in the upper part of the HZ (Figure 5). This would suppress the amount of NO_3^- entering the HZ by increasing the dispersive flux out from the SWI $\left(\left[NO_3^-\right]_{dspout}\right)$, where the incremental increase in $\left[NO_3^-\right]_{dspout}$ is larger than the incremental increase of advective flux of NO_3^- into the sediment $\left(\left[NO_3^-\right]_{advin}\right)$ resulting from temperature change (which in turn is due to increased hydraulic conductivity due to viscosity effects) as the temperature is higher than 25°C (Table 4). For example, as the temperature increased from 25°C to 30°C, $\left[NO_3^-\right]_{dspout}$ increased from 1.5×10^{-3} mg/(m s) to 3.6×10^{-3} mg/(m s); its net increase is 2.1×10^{-3} mg/(m s). $\left[NO_3^-\right]_{advin}$ increased from 1.3×10^{-2} mg/(m s) to 1.4×10^{-2} mg/(m s); its net increase is 1.0×10^{-3} mg/(m s) which is smaller than that of $\left[NO_3^-\right]_{dspout}$ (Table 4).

The trend of $\left[NO_3^-\right]_{in}$ in the pristine stream case, where it monotonically increased with increasing temperature (Table 5), is very different from that of the polluted stream case. Even though the NO_3^- production increased with temperature (Table 5), which should consequently inhibit the amount of nitrate entering into the HZ by enhancing $\left[NO_3^-\right]_{dspout}$, the incremental increase in $\left[NO_3^-\right]_{dspout}$ did not compensate for the incremental increase in $\left[NO_3^-\right]_{advin}$ due to the temperature change (Table 5).

As for N_A, for the polluted stream case, N_A increased initially and dropped off later on with further increasing temperature (Tables 4). For the pristine stream case, N_A monotonically increased with increasing temperature. In fact, both nitrification and denitrification rates rose as temperature went up (Tables 4 and 5). Because the relative concentration of NH_4^+ compared to NO_3^- is higher in the polluted stream case (Table 2), the nitrification rate is more sensitive to temperature in the polluted case than in the pristine case.

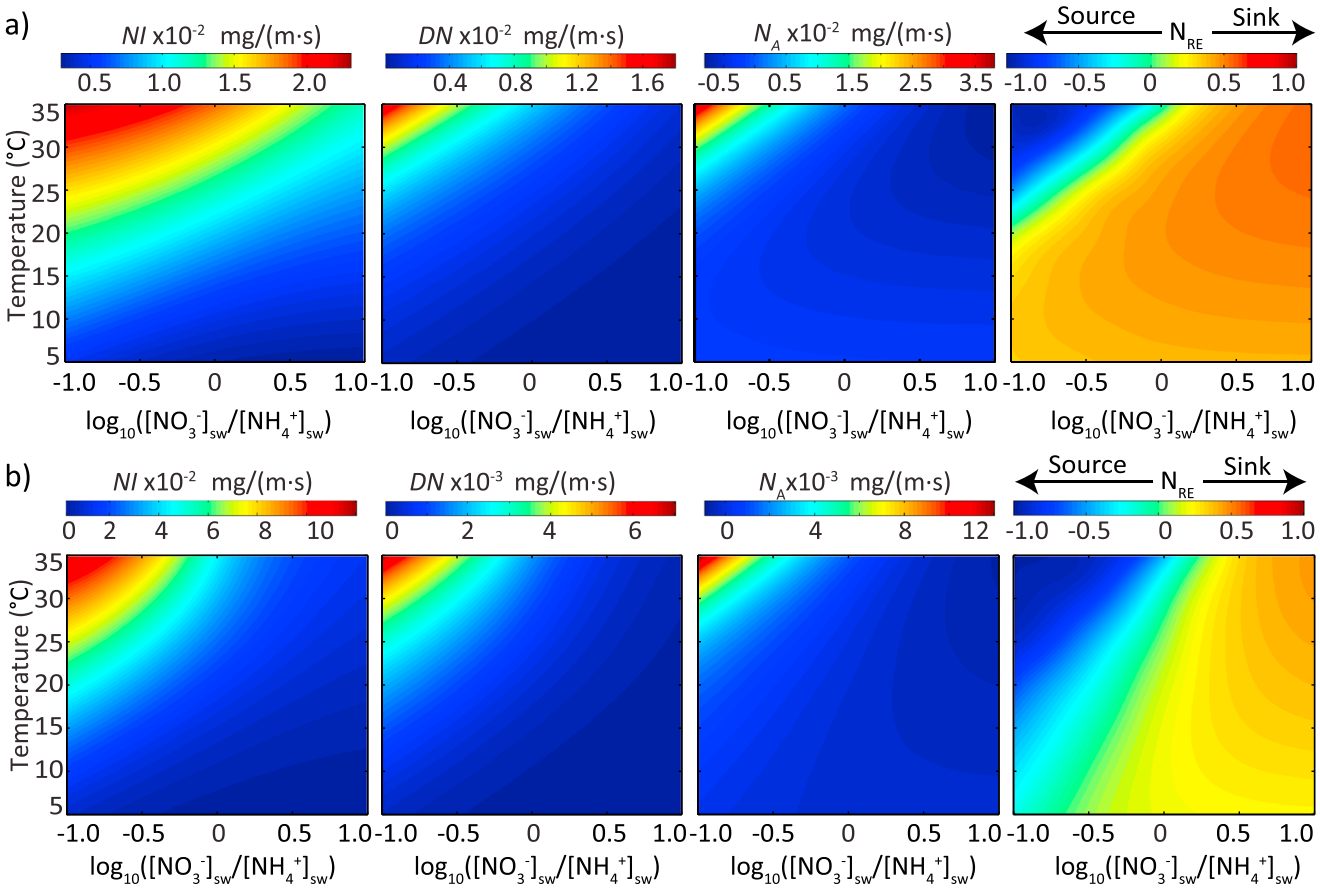

Figure 7. Sensitivity analysis for area-integrated nitrification NI, denitrification DN, net denitrification N_A, and removal efficiency N_{RE} with different ratios of $[NO_3^-]$ to $[NH_4^+]$ for the (a) polluted and (b) pristine stream cases.

We surmise that the difference in trends in N_A and N_{RE} with increasing temperatures can be ascribed to the differing availability of NH_4^+ and NO_3^- (Tables 4 and 5). This is a natural result of equation (7) which assumes direct and strong dependence of the nitrification rate on $[NH_4^+]$. Additionally, since DOC is present in sufficient amounts in both water quality scenarios, the denitrification rate is also highly sensitive to NO_3^- availability following equations 4–6. Therefore, the change in nitrification and denitrification rates is largely dependent on the relative amount of nitrate and ammonium. In order to further test this interpretation, we carried out a sensitivity analysis of varying $[NO_3^-]/[NH_4^+]$) and analyze its impact on N_A and N_{RE}.

4.2. Sensitivity Analysis of $[NO_3^-]/[NH_4^+]$ to Nitrate Removal and Production Efficiency

We implemented two sensitivity analyses by varying the ratio $[NO_3^-]/[NH_4^+]$ based on the initial concentration of both polluted and pristine cases (Table 2), respectively. Since we hypothesize that the relative amount of NO_3^- and NH_4^+ could affect the dependence of N_A and N_{RE} on temperature, we changed either $[NO_3^-]$ or $[NH_4^+]$ to alter the ratio ($[NO_3^-]/[NH_4^+]$). However, since the results were not sensitive to what species concentration is changing (results are not shown here), for simplicity, we only show results from changing $[NH_4^+]$ for both sensitivity cases, and we kept $[NO_3^-]$ constant.

In the sensitivity analysis, the logarithm of ($[NO_3^-]/[NH_4^+]$) ranged from −1 to 1 (Figure 7) in both cases, as the $[NH_4^+]$ was increased from 0.8 mg/L to 80 mg/L for the polluted stream sensitivity study, while the $[NH_4^+]$ was increased from 0.1 mg/L to 10 mg/L for the pristine stream sensitivity analysis. The temperature, as previously, was increased from 5°C to 35°C. For both stream cases, area-integrated nitrification and denitrification over the HZ increased as temperature increased (Figure 7). However, at higher $[NO_3^-]/[NH_4^+]$ ratio, N_A was negative (denitrification dominant), and its absolute value increased initially but reached its maximum value at a temperature then dropped off with further increasing temperature. That is, the maximum

nitrate removal rate occurs at higher $[NO_3^-]/[NH_4^+]$ ratio and moderate temperature. In addition, the optimal temperature for the maximum nitrate removal rate increased with the $[NO_3^-]/[NH_4^+]$ ratio. At lower $[NO_3^-]/[NH_4^+]$ ratio, for the polluted stream, N_A changed from negative value to positive value; for the pristine stream, N_A was positive across the entire temperature range (nitrification dominant), and its value increased as temperature increased. This supports our hypothesis that $[NO_3^-]/[NH_4^+]$ ratio is also an important factor affecting the temperature effect on nitrate removal ability (N_A) in the HZ.

With regard to N_{RE}, for both cases, at high $[NO_3^-]/[NH_4^+]$, the HZ functioned as a NO_3^- sink ($0 < N_{RE} < 1$), and the nitrate removal efficiency increased with increasing temperature (Figure 7). At lower $[NO_3^-]/[NH_4^+]$, the HZ behaved differently for the two scenarios. For the polluted stream, the HZ is a NO_3^- sink at low temperature but then switched to a NO_3^- source ($-1 < N_{RE} < 0$) as temperature went up. However, for the pristine stream, the HZ was always a NO_3^- source, and the NO_3^- production efficiency increased as temperature increased.

For both cases, there is a transitional range of $[NO_3^-]/[NH_4^+]$ where N_{RE} is very close to 0, and thus, it may fluctuate about 0, potentially causing the switching of HZ source-sink functionality with subtle temperature changes. The concentration ratio of the polluted stream case lies within the transitional range of $[NO_3^-]/[NH_4^+]$ (Table 2); therefore, the results are consistent with what the sensitivity analysis revealed. That is, the N_{RE} increased first as temperature went up, reached a maximum value, and then began to decline with further increasing temperature. Although the absolute ranges for the NO_3^- sink zone, the transition zone, and the NO_3^- source zone are different in these two sensitivity cases (Figure 7), the similar overall trend supports our interpretation of strong dependence on the $[NO_3^-]/[NH_4^+]$ ratio. This highlights the important contribution of $[NO_3^-]/[NH_4^+]$ to the influence of temperature on N_{RE}.

The sensitivity analysis (Figure 7) further illustrates the importance and interacting effects of stream temperature and stream water quality on HZ NO_3^- removal and production efficiency. It also revealed the important role of the relative supply of NH_4^+ compared to that of NO_3^- on N_A and N_{RE}.

4.3. Biogeochemical and Ecological Implications

Many previous studies have shown that hyporheic temperatures vary both temporally and spatially due to daily and seasonal changes in stream temperature and hyporheic exchange patterns [*Cardenas and Wilson*, 2007b; *Marzadri et al*., 2013; *Norman and Cardenas*, 2014; *Sharma et al*., 2012]. The results of our sensitivity analysis (Figure 7) indicate that during warmer temperatures, such as in summer at the seasonal scale or during daytime at the daily scale, nitrate removal (or production) efficiency would be higher compared to that in winter or at night. Whether the hyporheic zone acts as a nitrate source or sink also depends strongly on the $[NO_3^-]/[NH_4^+]$ of stream water. At high ratios, the HZ functions as a NO_3^- sink, nitrate removal efficiency increases as the temperature goes up. At intermediate or low ratios, the HZ functions as a NO_3^- source, nitrate production efficiency increases with increasing temperature, or the HZ may switch between a N sink during cooler periods and source during warmer periods even with and solely due slight temperature variation that might be observed within diurnal timescales (~5–10°C variation). Seasonal changes in temperature (say > 10°C) would lead to more pronounced changes in N cycling with increased N removal efficiency during the summer. Further, the thermal patchiness of HZs, particularly in stream reaches that are gaining groundwater with potentially different temperatures, might also translate to N removal efficiency patchiness. Thus, our results imply that field and laboratory studies of biogeochemical reactions in the HZ are further confounded by the stream and hyporheic thermal regimes.

4.4. Limitations of This Study and Future Directions

While this study is one of the first to couple and integrate fluid flow and reactive solute transport while relating the biogeochemical reactions to temperature, our analysis did not consider dynamic changes in hyporheic temperature and its potentially complex effect on transient biogeochemical reactions. All the flow models were steady state, assumed homogeneous sediment, and also assumed thermal homogeneity throughout the domain. We did not consider the effect of ambient groundwater flow and solute inputs and sediment sorption in this study. Furthermore, stream DO concentration decreases with increasing temperature [*Veraart et al*., 2011]. We did not consider this thermal effect on stream DO concentration in order to isolate and focus on the temperature effect on N cycling. In general, all stream solute concentrations were

kept constant in time, whereas these may vary in certain real field situations. Future studies should focus on simultaneously varying these parameters through space and time. In addition, this study focused on a single dune geometry and a single value of dispersivity. These factors could influence hyporheic exchange which drives advection of solute mass and energy, thus affecting the solute mass and thermal distribution and corresponding chemical reactions. Future studies should focus on more realistic, complex bed forms considering the superimposition of smaller bed forms upon larger ones and could conduct a sensitivity analysis on dispersivity. The above aspects are beyond the scope of this current study which provides the foundation for future investigations. Nonetheless, our results shed light on temperature effects on nitrogen cycling.

5. Summary and Conclusions

Hyporheic zones are hot spots for N transformations and affect the fate of N in aquatic systems. Biogeochemical reactions in the HZ are naturally complicated by the interaction and competition between the supply rate of reactants, temperature changes, hydraulic properties of the sediment, hydrodynamics of the river, and morphology of the bed. A better understanding of how these factors affect N would be beneficial for predicting the reduction and production of N from the laboratory scale to the field scale, which could potentially be extrapolated to the watershed scale. Due to the complex interactions of the enumerated factors, this study focused on and isolated the effects of temperature. We conducted a series of numerical simulations which considered turbulent open channel flow, pore water flow, and reactive transport models with temperature-dependent reaction constants via the Arrhenius equation. Different homogeneous and steady temperatures were implemented to study the effect of temperature on the hyporheic NO_3^- source/sink function and its associated efficiency. We found that while interfacial fluid flux across the SWI expectedly increased with increasing temperature, the total flux of nitrate from the river into HZ does not always follow the same increasing trend. The relative amount of nitrate and ammonium in the stream, which entered the HZ, also determined whether the HZ functions as a nitrate source or sink, as well as its efficiency in producing or consuming nitrate. Thus, our model results show that water temperature and $[NO_3^-]/[NH_4^+]$ in the stream are both other potentially critical parameters controlling the HZ nitrate removal or production efficiency. There are multiple factors and mutual coupling that result in the complex temperature dependence of reaction rates. N transformation reaction rates are heavily dependent on temperature, but simply using the Arrhenius equation to predict the reaction rate would lead to incomplete insight by ignoring the changes in interfacial fluid flux and reaction areas. The knowledge gained from this study highlights the importance of temperature effect on nitrogen cycling; it would guide the prediction and management of stream water quality and ecosystems. Future directions should extend the models to include couple dynamic temperatures and reactive solute transport in order to further understand the variable stream water temperature effect on the fate of nutrients and hyporheic nitrate source/sink function.

Acknowledgments
This research was supported by the National Science Foundation (EAR-0955750) and the Geology Foundation at the University of Texas at Austin. All data for this paper are properly cited and referred to in the reference list. There are no data sharing issue because all results retrieved from numerical simulations are provided in the figures and table. We thank Jud Harvey for his helpful reviews; an anonymous reviewer is also acknowledged.

References

Alexander, R. B., R. A. Smith, and G. E. Schwarz (2000), Effect of stream channel size on the delivery of nitrogen to the Gulf of Mexico, *Nature*, *403*(6771), 758–761, doi:10.1038/35001562.

Alexander, R. B., J. K. Böhlke, E. W. Boyer, M. B. David, J. W. Harvey, P. J. Mulholland, S. P. Seitzinger, C. R. Tobias, C. Tonitto, and W. M. Wollheim (2009), Dynamic modeling of nitrogen losses in river networks unravels the coupled effects of hydrological and biogeochemical processes, *Biogeochemistry*, *93*(1–2), 91–116, doi:10.1007/s10533-008-9274-8.

Bardini, L., F. Boano, M. B. Cardenas, R. Revelli, and L. Ridolfi (2012), Nutrient cycling in bedform induced hyporheic zones, *Geochim. Cosmochim. Acta*, *84*, 47–61, doi:10.1016/j.gca.2012.01.025.

Bardini, L., F. Boano, M. B. Cardenas, A. Sawyer, R. Revelli, and L. Ridolfi (2013), Small scale permeability heterogeneity has negligible effects on nutrient cycling in steambeds, *Geophys. Res. Lett.*, *40*, 1118–1122, doi:10.1002/grl.50224.

Birgand, F., R. W. Skaggs, G. M. Chescheir, and J. W. Gilliam (2007), Nitrogen removal in streams of agricultural catchments—A literature review, *Crit. Rev. Environ. Sci. Technol.*, *37*(5), 381–487, doi:10.1080/10643380600966426.

Boano, F., J. W. Harvey, A. Marion, A. I. Packman, R. Revelli, L. Ridolfi, and A. Wörman (2014), Hyporheic flow and transport processes: Mechanisms, models, and biogeochemical implications, *Rev. Geophys.*, *52*, 603–679, doi:10.1002/2012RG000417.

Boulton, A. J., S. Findlay, P. Marmonier, E. H. Stanley, and H. M. Valett (1998), The functional significance of the hyporheic zone in streams and rivers, *Annu. Rev. Ecol. Syst.*, *29*(1), 59–81.

Brunke, M., and T. Gonser (1997), The ecological significance of exchange processes between rivers and groundwater, *Freshwater Biol.*, *37*(1), 1–33, doi:10.1046/j.1365-2427.1997.00143.x.

Cardenas, M. B. (2008), The effect of river bend morphology on flow and timescales of surface water–groundwater exchange across pointbars, *J. Hydrol.*, *362*(1–2), 134–141, doi:10.1016/j.jhydrol.2008.08.018.

Cardenas, M. B. (2015), Hyporheic zone hydrologic science: A historical account of its emergence and a prospectus, *Water Resour. Res.*, *51*, 3601–3616, doi:10.1002/2015WR017028.

Cardenas, M. B., and J. L. Wilson (2007a), Dunes, turbulent eddies, and interfacial exchange with permeable sediments, *Water Resour. Res.*, *43*, W08412, doi:10.1029/2006WR005787.

Cardenas, M. B., and J. L. Wilson (2007b), Effects of current-bed form induced fluid flow on the thermal regime of sediments, *Water Resour. Res.*, *43*, W08431, doi:10.1029/2006WR005343.
Cardenas, M. B., J. Wilson, and V. A. Zlotnik (2004), Impact of heterogeneity, bed forms, and stream curvature on subchannel hyporheic exchange, *Water Resour. Res.*, *40*, W08307, doi:10.1029/2004WR003008.
Cirmo, C. P., and J. J. McDonnell (1997), Linking the hydrologic and biogeochemical controls of nitrogen transport in near-stream zones of temperate-forested catchments: A review, *J. Hydrol.*, *199*(1), 88–120, doi:10.1016/S0022-1694(96)03286-6.
Clément, J.-C., G. Pinay, and P. Marmonier (2002), Seasonal dynamics of denitrification along topohydrosequences in three different riparian wetlands, *J. Environ. Qual.*, *31*(3), 1025–1037, doi:10.2134/jeq2002.1025.
Dawson, R., and K. Murphy (1972), The temperature dependency of biological denitrification, *Water Res.*, *6*, 71–83, doi:10.1016/0043-1354(72)90174-1.
Duff, J. H., and F. J. Triska (1990), Denitrifications in sediments from the hyporheic zone adjacent to a small forested stream, *Can. J. Fish. Aquat. Sci.*, *47*(6), 1140–1147.
Engler, R., and W. Patrick (1974), Nitrate removal from floodwater overlying flooded soils and sediments, *J. Environ. Qual.*, *3*(4), 409–413, doi:10.2134/jeq1974.00472425000300040025x.
Findlay, S. (1995), Importance of surface-subsurface exchange in stream ecosystems: The hyporheic zone, *Limnol. Oceanogr.*, *40*(1), 159–164, doi:10.4319/lo.1995.40.1.0159.
Galloway, J. N., J. D. Aber, J. W. Erisman, S. P. Seitzinger, R. W. Howarth, E. B. Cowling, and B. J. Cosby (2003), The nitrogen cascade, *BioScience*, *53*(4), 341–356, doi:10.1641/0006-3568.
Gomez-Velez, J. D., J. W. Harvey, M. B. Cardenas, and B. Kiel (2015), Denitrification in the Mississippi River network controlled by flow through river bedforms, *Nat. Geosci.*, *8*, 941–945, doi:10.1038/ngeo2567.
Groffman, P. M., A. M. Dorsey, and P. M. Mayer (2005), N processing within geomorphic structures in urban streams, *J. North Am. Benthol. Soc.*, *24*, 613–625, doi:10.1899/04-026.1.
Harvey, J. W., and M. Gooseff (2015), River corridor science: Hydrologic exchange and ecological consequences from bedforms to basins, *Water Resour. Res.*, *51*, 6893–6922, doi:10.1002/2015WR017617.
Harvey, J. W., J. K. Böhlke, M. A. Voytek, D. Scott, and C. R. Tobias (2013), Hyporheic zone denitrification: Controls on effective reaction depth and contribution to whole-stream mass balance, *Water Resour. Res.*, *49*, 6298–6316, doi:10.1002/wrcr.20492.
Howard-Williams, C., S. Pickmere, and J. Davies (1983), Decay rates and nitrogen dynamics of decomposing watercress (Nasturtium officinale R. Br.), *Hydrobiologia*, *99*(3), 207–214, doi:10.1007/BF00008772.
Hunter, K. S., Y. Wang, and P. Van Cappellen (1998), Kinetic modeling of microbially-driven redox chemistry of subsurface environments: Coupling transport, microbial metabolism and geochemistry, *J. Hydrol.*, *209*(1), 53–80, doi:10.1016/S0022-1694(98)00157-7.
Janssen, F., M. B. Cardenas, A. H. Sawyer, T. Dammrich, J. Krietsch, and D. Beer (2012), A comparative experimental and multiphysics computational fluid dynamics study of coupled surface–subsurface flow in bed forms, *Water Resour. Res.*, *48*, W08514, doi:10.1029/2012WR011982.
Jones, J. B., Jr., and R. M. Holmes (1996), Surface-subsurface interactions in stream ecosystems, *Trends Ecol. Evol.*, *11*(6), 239–242, doi:10.1016/0169-5347(96)10013-6.
Jones, J. B., Jr., S. G. Fisher, and N. B. Grimm (1995), Nitrification in the hyporheic zone of a desert stream ecosystem, *J. North Am. Benthol. Soc.*, *14*, 249–258, doi:10.2307/1467777.
Kaushik, N., and J. Robinson (1976), Preliminary observations on nitrogen transport during summer in a small spring-fed Ontario stream, *Hydrobiologia*, *49*(1), 59–63, doi:10.1007/BF00016169.
Kessler, A. J., M. B. Cardenas, I. R. Santos, and P. L. M. Cook (2014), Enhancement of denitrification in permeable carbonate sediment due to intra-granular porosity: A multi-scale modelling analysis, *Geochim. Cosmochim. Acta*, *141*, 440–453, doi:10.1016/j.gca.2014.06.028.
Kiel, B. A., and M. B. Cardenas (2014), Lateral hyporheic exchange throughout the Mississippi River network, *Nat. Geosci.*, *7*(6), 413–417, doi:10.1038/ngeo2157.
Martin, L. A., P. J. Mulholland, J. R. Webster, and H. M. Valett (2001), Denitrification potential in sediments of headwater streams in the southern Appalachian Mountains, USA, *J. North Am. Benthol. Soc.*, *20*(4), 505–519, doi:10.2307/1468084.
Marzadri, A., D. Tonina, and A. Bellin (2012), Morphodynamic controls on redox conditions and on nitrogen dynamics within the hyporheic zone: Application to gravel bed rivers with alternate-bar morphology, *J. Geophys. Res.*, *117*, G00N10, doi:10.1029/2012JG001966.
Marzadri, A., D. Tonina, and A. Bellin (2013), Quantifying the importance of daily stream water temperature fluctuations on the hyporheic thermal regime: Implication for dissolved oxygen dynamics, *J. Hydrol.*, *507*, 241–248, doi:10.1016/j.jhydrol.2013.10.030.
McClain, M. E., E. W. Boyer, C. L. Dent, S. E. Gergel, N. B. Grimm, P. M. Groffman, S. C. Hart, J. W. Harvey, C. A. Johnston, and E. Mayorga (2003), Biogeochemical hot spots and hot moments at the interface of terrestrial and aquatic ecosystems, *Ecosystems*, *6*(4), 301–312, doi:10.1007/s10021-003-0161-9.
Norman, F. A., and M. B. Cardenas (2014), Heat transport in hyporheic zones due to bedforms: An experimental study, *Water Resour. Res.*, *50*, 3568–3582, doi:10.1002/2013WR014673.
Packman, A. I., and M. Salehin (2003), Relative roles of stream flow and sedimentary conditions in controlling hyporheic exchange, *Hydrobiologia*, *494*(1), 291–297, doi:10.1023/A:1025403424063.
Peterson, B. J., W. M. Wollheim, P. J. Mulholland, J. R. Webster, J. L. Meyer, J. L. Tank, E. Martí, W. B. Bowden, H. M. Valett, and A. E. Hershey (2001), Control of nitrogen export from watersheds by headwater streams, *Science*, *292*(5514), 86–90, doi:10.1126/science.1056874.
Sawyer, A. H., M. B. Cardenas, and J. Buttles (2011), Hyporheic exchange due to channel-spanning logs, *Water Resour. Res.*, *47*, W08502, doi:10.1029/2011WR010484.
Sawyer, A. H., M. B. Cardenas, and J. Buttles (2012), Hyporheic temperature dynamics and heat exchange near channel-spanning logs, *Water Resour. Res.*, *48*, W01529, doi:10.1029/2011WR011200.
Schmidt, E. (1979), *Properties of Water and Steam in SI-Units*, Springer, New York.
Sharma, L., J. Greskowiak, C. Ray, P. Eckert, and H. Prommer (2012), Elucidating temperature effects on seasonal variations of biogeochemical turnover rates during riverbank filtration, *J. Hydrol.*, *428*, 104–115, doi:10.1016/j.jhydrol.2012.01.028.
Sheibley, R. W., A. P. Jackman, J. H. Duff, and F. J. Triska (2003), Numerical modeling of coupled nitrification–denitrification in sediment perfusion cores from the hyporheic zone of the Shingobee River, MN, *Adv. Water Resour.*, *26*(9), 977–987, doi:10.1016/S0309-1708(03)00088-5.
Stanford, J. A., and J. V. Ward (1988), The hyporheic habitat of river ecosystems, *Nature*, *335*(6185), 64–66, doi:10.1038/335064a0.
Svendsen, L. M., and B. Kronvang (1993), Retention of nitrogen and phosphorus in a Danish lowland river system: Implications for the export from the watershed, in *Nutrient Dynamics and Retention in Land/Water Ecotones of Lowland, Temperate Lakes and Rivers*, edited by A. Hillbricht-Ilkowska and E. Pieczynska, pp. 123–135, Springer, Netherlands, doi:10.1007/978-94-011-1602-2_15.

Swanson, T. E., and M. B. Cardenas (2010), Diel heat transport within the hyporheic zone of a pool-riffle-pool sequence of a losing stream and evaluation of models for fluid flux estimation using heat, *Limnol. Oceanogr.*, *55*(4), 1741–1754, doi:10.4319/lo.2010.55.4.1741.

Thamdrup, B., J. W. Hansen, and B. B. Jørgensen (1998), Temperature dependence of aerobic respiration in a coastal sediment, *FEMS Microbiol. Ecol.*, *25*(2), 189–200, doi:10.1111/j.1574-6941.1998.tb00472.x.

Veraart, A. J., J. J. M. de Klein, and M. Scheffer (2011), Warming can boost denitrification disproportionately due to altered oxygen dynamics, *PLoS One*, *6*(3), e18508, doi:10.1371/journal.pone.0018508.

Wilcox, D. (1991), A half century historical review of the k-w model, AIAA 91-0615.

Yvon-Durocher, G., et al. (2012), Reconciling the temperature dependence of respiration across timescales and ecosystem types, *Nature*, *487*(7408), 472–476, doi:10.1038/nature11205.

Zarnetske, J. P., R. Haggerty, S. M. Wondzell, and M. A. Baker (2011a), Dynamics of nitrate production and removal as a function of residence time in the hyporheic zone, *J. Geophys. Res.*, *116*, G01025, doi:10.1029/2010JG001356.

Zarnetske, J. P., R. Haggerty, S. M. Wondzell, and M. A. Baker (2011b), Labile dissolved organic carbon supply limits hyporheic denitrification, *J. Geophys. Res.*, *116*, G04036, doi:10.1029/2011JG001730.

Zarnetske, J. P., R. Haggerty, S. M. Wondzell, V. A. Bokil, and R. González-Pinzón (2012), Coupled transport and reaction kinetics control the nitrate source-sink function of hyporheic zones, *Water Resour. Res.*, *48*, W11508, doi:10.1029/2012WR011894.